

Diffusive domain coarsening: Early time dynamics and finite-size effects

Suman Majumder and Subir K. Das*

Theoretical Sciences Unit, Jawaharlal Nehru Centre for Advanced Scientific Research, Jakkur P.O., Bangalore 560064, India

(Received 24 January 2011; revised manuscript received 21 March 2011; published 5 August 2011)

We study the diffusive dynamics of phase separation in a symmetric binary (A + B) mixture with a 50:50 composition of A and B particles, following a quench below the demixing critical temperature, both in spatial dimensions $d = 2$ and $d = 3$. The particular focus of this work is to obtain information about the effects of system size and correction to the growth law via the appropriate application of the finite-size scaling method to the results obtained from the Kawasaki exchange Monte Carlo simulation of the Ising model. Observations of only weak size effects and a very small correction to scaling in the growth law are significant. The methods used in this work and information thus gathered will be useful in the study of the kinetics of phase separation in fluids and other problems of growing length scale. We also provide a detailed discussion of the standard methods of understanding simulation results which may lead to inappropriate conclusions.

DOI: [10.1103/PhysRevE.84.021110](https://doi.org/10.1103/PhysRevE.84.021110)

PACS number(s): 64.60.Ht, 64.70.Ja

I. INTRODUCTION

When a homogeneous binary mixture (A + B) is quenched inside the miscibility gap, the system falls out of equilibrium and moves toward its new equilibrium state via the formation and growth of domains rich in A or B particles [1–3]. This coarsening of domains is a scaling phenomenon, e.g., the two-point equal-time correlation function $C(r, t)$, the structure factor $S(k, t)$, and the domain size distribution function $P(\ell_d, t)$ obey the scaling relations

$$C(r, t) \equiv \tilde{C}[r/\ell(t)], \quad (1)$$

$$S(k, t) \equiv \ell(t)^d \tilde{S}[k\ell(t)], \quad (2)$$

$$P(\ell_d, t) \equiv \ell(t)^{-1} \tilde{P}[\ell_d/\ell(t)], \quad (3)$$

where the average domain size $\ell(t)$ increases with time (t) in a power-law fashion,

$$\ell(t) \sim t^\alpha, \quad (4)$$

and $\tilde{C}(x)$, $\tilde{S}(y)$, and $\tilde{P}(z)$ are scaling functions independent of $\ell(t)$. In Eq. (4), the growth exponent α depends upon the transport mechanism.

For diffusive growth, by associating the rate of increase of $\ell(t)$ with the chemical potential (μ) gradient, one can write [1]

$$\frac{d\ell(t)}{dt} \sim |\vec{\nabla}\mu| \sim \frac{\sigma}{\ell(t)^2}, \quad (5)$$

with σ being the A-B interfacial tension. The solution of Eq. (5) gives $\alpha = 1/3$, which is known as the Lifshitz-Sloyozov (LS) law [4]. The LS behavior is the only asymptotic growth law expected for phase-separating solid mixtures. However, for fluids and polymers, one expects faster growth at large length scales where hydrodynamic effects are dominant. For the latter, in $d = 3$, convective transport yields additional growth regimes [5,6] with

$$\begin{aligned} \alpha &= 1, & \ell(t) \ll \ell_{\text{in}}, \\ \alpha &= 2/3, & \ell(t) \gg \ell_{\text{in}}. \end{aligned} \quad (6)$$

In Eq. (6), the inertial length $\ell_{\text{in}} \simeq \eta^2/(\rho\sigma)$, with η and ρ being the shear viscosity and mass density, respectively, marks the crossover from a low-Reynold-number viscous hydrodynamic regime to an inertial regime.

In this work, we have undertaken a comprehensive study to learn about the finite-size effects in domain coarsening in the Ising model with conserved order parameter dynamics and to understand the behavior of the growth exponent as a function of time, via the application of the finite-size scaling method [7,8] both in space dimensions $d = 2$ and $d = 3$. While originally developed to understand simulations in equilibrium critical phenomena, the finite-size scaling method has found interesting applications [9–11] in nonequilibrium processes as well. In this paper, we exploit this method appropriately in the context of diffusive phase-separation kinetics to show that for critical quench, the LS value of α sets in very early and the effect of size is very small.

Diffusive domain coarsening in solid binary mixtures has been extensively studied via the Ising model,

$$H = -J \sum_{\langle ij \rangle} S_i S_j; \quad S_i = \pm 1, \quad J > 0, \quad (7)$$

which is the prototype for a large class of critical phase transitions. Here one can identify the spin $S_i = +1$ (-1) at lattice site i with an A particle (B particle). Note that $\langle ij \rangle$ in Eq. (7) stands for the summation over only the nearest neighbors. One can also study the kinetics of phase separation via dynamical equations, which can be obtained from Ising models in a mean field approximation by using a master equation approach [12,13] with Kawasaki exchange kinetics [14]. Upon coarse graining, such equations lead to the Cahn-Hilliard (CH) equation

$$\frac{d\psi(\vec{r}, t)}{dt} = -\nabla^2 [\psi(\vec{r}, t) + \nabla^2 \psi(\vec{r}, t) - \psi^3(\vec{r}, t)], \quad (8)$$

where $\psi(\vec{r}, t)$ is a coarse-grained, time-dependent local order parameter. Note that such a continuum description could also be obtained in a phenomenological manner [1,15] using a coarse-grained Ginzburg-Landau (GL) free energy functional with the requirement of conservation of material. The CH equation with an added thermal noise is expected to be

*das@jncasr.ac.in

equivalent to the Monte Carlo (MC) simulations [16,17] of kinetic Ising models.

In Eq. (8), the typical distance over which the order parameter is coarse grained is of the size of equilibrium correlation length ξ . In situations when one is interested in studying the kinetics in the close vicinity of the critical point, without focusing on the dynamics at a microscopic level, Eq. (8) is computationally very useful in achieving the asymptotic [18] behavior. However, for deep quenches, one needs to incorporate higher order terms than are usually used in the GL Hamiltonian. Also, at very low temperature, where ξ is of the order of a lattice constant, the CH equation would not provide information of a large effective system size compared to the atomistic Ising model. The particular focus of this work is to learn the finite-size effects and dynamics at the early stage, both of which have received much less attention compared to the identification of domain growth law in the long-time limit, despite their obvious importance both fundamentally and technologically, e.g., in nanoscience and technology. In view of this, we choose to revisit the kinetics of phase separation in the Ising model via MC simulations.

While MC simulations have been used immensely in the understanding of nonequilibrium domain growth phenomena, both with conserved [9,10,19–24] and nonconserved [10,25,26] order parameter, earlier studies of phase ordering in a conserved Ising model with critical (50:50) composition reported [27,28] estimates of $\alpha \in [0.17, 0.25]$, deviating drastically from the expected LS law. Even arguments in favor of logarithmic growth were proposed [29]. Note that these earlier reports were based on MC simulations for very short periods of time, where contamination of domain structures due to thermal noise might not have been taken care of, which could act as a source of significant error in the measurement of average domain size.

Later, the discrepancy of the previous results with the expected LS behavior was understood to be due to strong corrections to scaling at early time. To account for this [20], higher order terms in Eq. (5) were incorporated to write

$$\frac{d\ell(t)}{dt} = \frac{C_1}{\ell(t)^2} + \frac{C_2}{\ell(t)^3} + O[\ell(t)^{-4}], \quad (9)$$

which in the long-time limit gives a solution $\propto t^{1/3}$; however, would give rise to a leading order correction linear in $1/\ell(t)$ to the instantaneous exponent. Thus LS behavior will be observed only in the limit $\ell(t \rightarrow \infty) \rightarrow \infty$. Indeed, consistency with a linear correction was observed for a 50:50 binary mixture [20, 21], as well as for multicomponent mixtures [24]. The present work, however, convincingly demonstrates that the observation of the LS value of the exponent only in the asymptotic limit was misleading, and the presence of a time-independent bare length in $\ell(t)$ is responsible for the numerical data exhibiting such a trend.

Most of the studies to date have stressed the use of large systems, with the anticipation of strong finite-size effects [30] combined with the expectation that the LS law will be realized only in the large $\ell(t)$ limit. This strategy, of course, will prove to be useful when there is dynamical crossover, as in domain coarsening in fluids [cf. Eq. (6)], where the system size should be significantly larger than the smallest characteristic length scale in a particular regime. However,

consideration of arbitrarily large system sizes restricts the access of a large time scale, particularly for the molecular dynamics simulation of fluid phase separation [31–33]. It is worth mentioning that the typical system sizes that authors consider nowadays contain a number of lattice sites or particles of the order of a million, which is too large even for present day computers to access the long-time scale that often is a necessity. Such choice of large systems, in addition to the anticipation of a strong finite-size effect, was often motivated by the expectation of better self-averaging [30], which is an issue [25] that needs further attention to be resolved. Thus a judicious choice of system sizes is very crucial for such problems [34], which in turn requires appropriate knowledge of finite-size effects [11]. While recent focus has been on more complicated systems [35–42] with realistic interactions and physical boundary conditions, much basic information as discussed above is lacking, even in a situation as simple as Ising systems.

This paper is organized as follows. In Sec. II, we describe the details of the simulation and finite-size scaling method. Results for both $d = 2$ and $d = 3$ are presented in Sec. III, while Sec. IV summarizes the paper with a discussion of future possibilities in this direction.

II. METHODS

A. Details of simulation and calculation of observables

In the MC simulation of the Ising model, the conserved order-parameter dynamics, where the composition of up (A particle) and down (B particle) spins remains fixed during the entire evolution, is implemented via the standard Kawasaki exchange mechanism [14], where the interchange of positions between a randomly chosen pair of nearest neighbor (nn) spins comprises a trial move. A move is accepted or rejected according to the standard Metropolis algorithm [16]. One MC step (MCS) consists of exchange trials over L^d pairs of spins, with L being the linear dimension of a square (cubic) system. Periodic boundary conditions were applied in all directions.

Note that with the increase of temperature, the accurate measurement of average domain size becomes difficult due to the presence of noisy clusters of the size of $\xi(T)$. On the other hand, at very low temperature, growth is hampered by metastability. To avoid the latter problem, we have set the temperature toward the higher side and calculated all of the physical quantities from pure domain morphology after eliminating the thermal noise via a majority spin rule. There a spin at a lattice site i was replaced by the sign of the majority of the spins sitting at i and at nn of i (depending upon the noise level, i.e., the average size of noise clusters, extension to distant neighbors may also become necessary). In Fig. 1, we demonstrate such a filtering process for a rather high temperature. The left panel corresponds to the original snapshot from the MC simulation on a $2-d$ square lattice at $T = 0.85T_c$ with $L = 64$ at $t = 5 \times 10^3$ MCS. One can appreciate that the presence of substantial noise elements here would give rise to a smaller value of $\ell(t)$ than the actual. The right panel of the figure shows the snapshot with pure domain morphology obtained after implementing the noise removal exercise described above. Of course, one should be

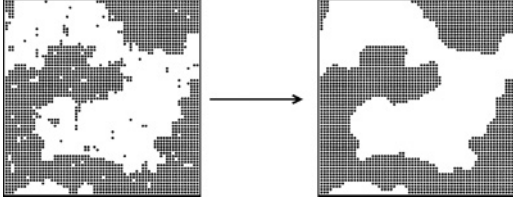


FIG. 1. Left panel: Snapshot of a 2- d Ising model at $T = 0.85T_c$ obtained from the Monte Carlo simulation via Kawasaki exchange kinetics, for $L = 64$ at $t = 5 \times 10^3$ MCS. Right panel: Same snapshot after removing the noise via the exercise described in the text. A particles are marked by black dots whereas B particles are unmarked.

careful that too many such iterations or consideration of very distant neighbors may alter the basic structure. However, in the present case, no such deformation has taken place. All the quantities in our simulation were calculated by using snapshots with a pure domain structure. In brief, the advantage of the above procedure could be understood in the following way. In most aging processes, fast quasi-equilibrium degrees of freedom coexist with slow nonequilibrium degrees, leading to an additive separation of the thermodynamic observables. Our method gets rid of the faster equilibrium degrees of freedom.

In Fig. 2(a), we present the scaling plots of domain size distribution function, viz., plots of $\ell(t)P(\ell_d, t)$ versus $\ell_d/\ell(t)$, where $\ell(t)$ was calculated from the first moment of the normalized distribution $P(\ell_d, t)$ as

$$\ell(t) = \int d\ell_d \ell_d P(\ell_d, t), \quad (10)$$

with length ℓ_d being obtained from the separation between the two successive interfaces (A and B domains) in the x , y , or z directions. Figures 2(b) and 2(c) show the scaling plots of the correlation function $C(r, t)$ and its Fourier transform $S(k, t)$, in accordance with Eqs. (1) and (2), where $C(r, t)$ was calculated as

$$C(r, t) = \langle S_i S_j \rangle, \quad r = |\vec{i} - \vec{j}|. \quad (11)$$

Note that these scaling plots for all the quantities were obtained by using the values of $\ell(t)$ obtained from Eq. (10). Of course, independently $\ell(t)$ could be calculated from the decay of $C(r, t)$, as well as the first moment of normalized $S(k, t)$ as

$$C[r = \ell(t), t] = h, \quad (12)$$

and

$$\ell(t) = \frac{1}{\int dk k S(k)}. \quad (13)$$

When calculated from a completely noise-free morphology, all of the above mentioned methods for the calculation of $\ell(t)$ must give results proportional to each other. When h is set to a rather small value, particularly when the decay length is larger than the average size of the noisy clusters, the calculation of $\ell(t)$ from Eq. (12) is not expected to be affected much by the presence of noise. The same applies for Eq. (13). However, when calculated via Eq. (10), either the distribution up to the length of the average noise size should be appropriately modified or noise should be completely eliminated. The latter

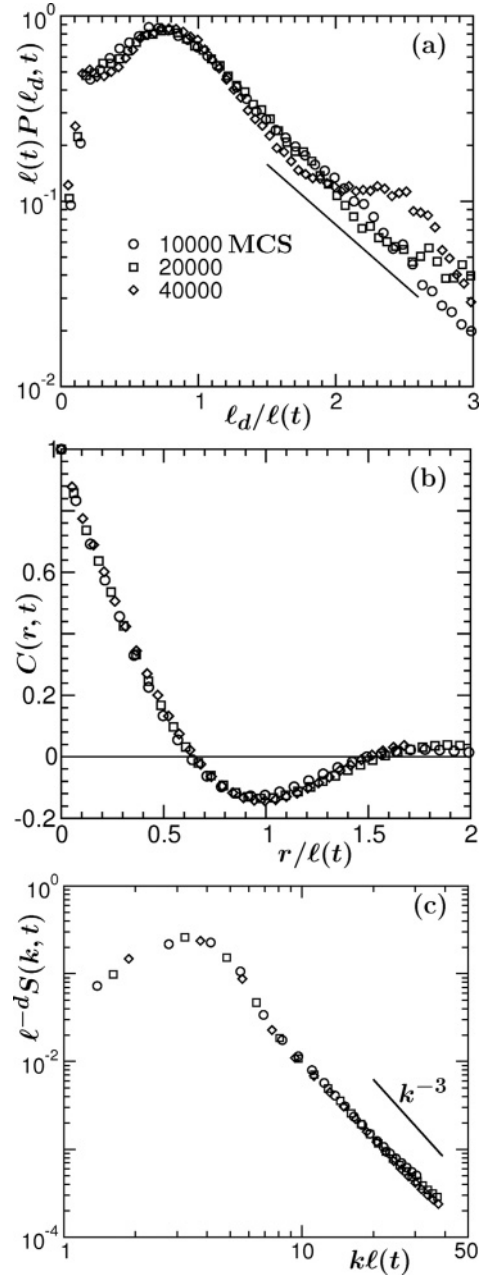


FIG. 2. Scaling plots of (a) domain size distribution $P(\ell_d, t)$, (b) correlation function $C(r, t)$, and (c) structure factor $S(k, t)$, from different times, as indicated, for the system in Fig. 1. The data were averaged over 50 independent initial configurations. Note that in all the cases, $\ell(t)$ used, was calculated using Eq. (10). While the solid line in (a) verifies exponential decay of the tail, the one in (c) corresponds to the Porod tail.

strategy is more appropriate, since it gives better shape to all the form functions. In our calculation, in Eq. (12), h will correspond to the first zero of $C(r, t)$.

All of the results presented in Fig. 2 are obtained from pure domain morphology and the nice data collapse obtained in each case using the measure of $\ell(t)$ from Eq. (10) speaks to the equivalence of all the definitions, given by Eqs. (10), (12), and (13). The linear behavior of the tail region in Fig. 2(a) on a semilogarithmic plot is consistent with an exponential decay

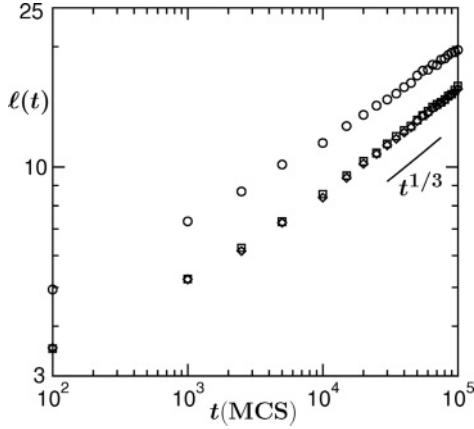


FIG. 3. Average domain size is plotted on a logarithmic scale as a function of time t . Different symbols correspond to the calculation of $\ell(t)$ from different quantities: circles from $P(\ell_d, t)$, squares from first zero-crossing of $C(r, t)$, diamonds from the first moment of $S(k, t)$. Results presented were obtained from the right panel of Fig. 1, with $L^2 = 128^2$ and $T = 0.85T_c$. The solid line corresponds to the theoretically expected $t^{1/3}$ behavior.

of $P(\ell_d, t)$. Here the noisy look (oscillatory behavior) at late time or large domain size limit (which was also observed in other recent studies [43,44]) is due to a lack of statistics when $\ell(t)$ becomes of the order of the system size. On the other hand, the linear look of large wave vector (k) data in Fig. 2(c) confirms the generalized Porod law [1,45,46]

$$S(k, t) \sim k^{-(d+n)}. \quad (14)$$

Note that in the present case, $d = 2$ and $n = 1$ (number of components of the order parameter). It is worth mentioning that one would have observed a slower decay of the structure factor had the noise not been removed.

In Fig. 3, we present the length scale results obtained from all of the above mentioned methods on a logarithmic scale, all of which look proportional to each other, as was also clear from the exercise of Fig. 2. The data at late times look consistent with the expected exponent $\alpha = 1/3$. Note that if the temperature is sufficiently close to T_c for a long enough time, the noise might not have equilibrated to the equilibrium value inside the true domains. In such a situation, the presence of two length scales in the problem may give rise to a misleading value of the exponent if the noise (equilibrium degree of freedom) is not eliminated and the range of fitting is small. Indeed a fitting of the data, obtained from the original snapshots (not shown), at temperature $0.85T_c$ to the form

$$\ell(t) = C + At^\alpha, \quad (15)$$

in the range $[0, 20000]$ MCS, gives $\alpha = [0.15, 0.25]$ [the value being larger when $\ell(t)$ is calculated from (12) or (13)], which is consistent with earlier reports [27,28]. On the other hand, a similar fitting to the data obtained after removing the noise gives $\alpha = [0.3, 0.34]$ and, within statistical deviation, does not depend upon the range of fitting. This latter result is already suggestive of the absence of a strong correction to the scaling. However, since data fitting is always not a very reliable exercise, as will be discussed later, to further substantiate the

claim about small correction to scaling, we take the route of a finite-size scaling analysis that will also be useful in quantifying the finite-size effect.

B. Formulation of finite-size scaling

In equilibrium critical phenomena, the singularity of a quantity Z is characterized in terms of $\epsilon = |T - T_c|$, the temperature deviation from the critical point, as

$$Z \approx Z_0 \epsilon^z \approx Z'_0 \xi^{-z/\nu}, \quad Z'_0 = Z_0 \xi_0^{z/\nu}, \quad (16)$$

where the correlation length ξ grows as

$$\xi \approx \xi_0 \epsilon^{-\nu}, \quad (17)$$

with z and ν being the critical exponents. However, for finite values of L , any critical enhancement is restricted and Z is smooth and analytic. Such finite-size effects may appear as a difficulty in understanding results from computer simulations. However, this problem can be tackled by writing down the finite-size scaling ansatz [7], thus accounting for the size effect, as

$$Z \approx Y(x) \epsilon^z = Y'(x) \xi^{-z/\nu}. \quad (18)$$

In Eq. (18), $Y(x)$ is the finite-size scaling function that depends upon the scaled variable $x = L/\xi$ and is independent of system size. Note that Y and Y' differ by a factor originating from the different amplitudes Z_0 and Z'_0 used in Eq. (16). In further discussion, however, we will remove the primes from both Z_0 and Y and a distinction can be derived from whether the scaling forms are written in terms of ϵ or ξ .

At this stage, it is important to ask about the behavior of Y as a function of x . While for static quantities such a question is already addressed, for dynamics, where the finite-size effects are found [47] to be much stronger, there is no appropriate understanding of the variation of $Y(x)$. Nevertheless, one can write down the following limiting behaviors:

$$\text{for } x \rightarrow 0 (\xi \rightarrow \infty; L < \infty), \quad Y(x) \sim x^{-z/\nu}, \quad (19)$$

such that Z is finite at criticality,

$$Z \sim L^{-z/\nu}. \quad (20)$$

Equation (20), when compared with Eq. (16), is consistent with the fact that the only important length in the problem at criticality is ξ , and it must scale with the varying system size L . Keeping this important fact in mind, in fact, one can write (18) as

$$Z \approx Y(x) L^{-z/\nu}. \quad (21)$$

On the other hand,

$$\text{for } x \rightarrow \infty (L \rightarrow \infty, \epsilon > 0), \quad Y(x) = Z_0, \quad (22)$$

so that Eq. (16) is recovered in the thermodynamic limit.

With the knowledge of ν , Eq. (20) can be used to estimate z by calculating Z at T_c for various system sizes. A better strategy, however, is to study Z at finite-size critical points T_c^L , such that

$$Z|_{T_c^L} \sim L^{-z/\nu}, \quad T_c^L - T_c \sim L^{-1/\nu}, \quad (23)$$

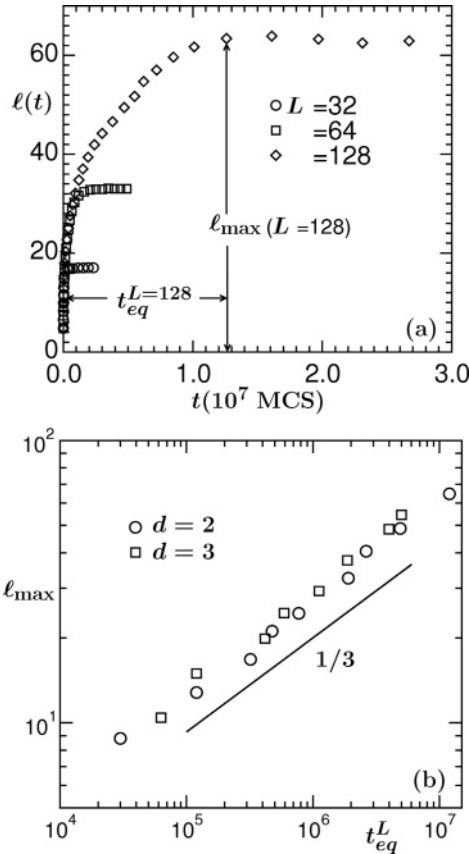


FIG. 4. (a) Plot of average domain size $\ell(t)$, obtained from Eq. (10), for the 2- d Ising model, for different system sizes (indicated on the figure) at $T = 0.6T_c$. Definitions of ℓ_{\max} and t_{eq}^L are demonstrated. Data for $L = 32$ and $L = 64$ were averaged over 1000 independent initial configurations, whereas only 40 different initial realizations were used for $L = 128$. Note that all subsequent results in this paper are obtained at the same temperature as this. (b) Demonstration of the scaling behavior (29) in $d = 2$ and 3.

although the true meaning of a critical point can be assigned to T_c^L only in the limit $L \rightarrow \infty$.

This general discussion about the finite-size scaling method could be used to construct the similar formalism for the nonequilibrium domain coarsening problem, where $\ell(t)$ is the variable analogous to ξ and $1/t$ is analogous to ϵ . In the present problem, $\ell(t)$ should scale with L , more precisely $\ell_{\max} \sim \ell(t)$, where $\ell_{\max}(L)$ is the equilibrium domain size and proportional to the system size L . In Fig. 4(a), we show plots of $\ell(t)$ versus t for various values of L , in $d = 2$. The flat regions in the plots at late times correspond to ℓ_{\max} .

At this stage, we would like to quantify the domain growth in an infinite system as

$$\ell(t') = \ell_0 + At'^\alpha, \quad (24)$$

where ℓ_0 is temperature dependent (as is the amplitude A) and could possibly be interpreted as the average cluster size when the system becomes unstable to fluctuations at time t_0 since the quench or the domain length at t_0 when the system enters the scaling regime. Of course our measurement of time starts from there, i.e., $t' = t - t_0$. Note that we are reluctant

to assign a meaning of domain size to this quantity and this should be treated in a manner similar to a background quantity in critical phenomena that appears from small length fluctuations whose temperature variation is usually neglected. Having said that, the scaling part in Eq. (24) is only At'^α . Of course, when $\ell(t')$ is significantly large, subtraction of the microscopic length ℓ_0 does not result in a noticeable difference. However, in computer simulations, where one deals with small systems, the presence of ℓ_0 can result in completely different conclusions.

Equation (24) is valid only in the absence of any finite-size effect. For a finite $\ell_{\max}(L)$, analogous to (18), one can write down the scaling ansatz as

$$\ell(t') - \ell_0 = Y(x)t'^\alpha, \quad (25)$$

where now

$$x = \frac{\ell_{\max} - \ell_0}{t'^\alpha} \quad (26)$$

is the scaling variable. In both Eqs. (25) and (26), ℓ_0 is subtracted to deal with the scaling parts only. By observing (16), (19), and (22), as well as (24), (25), and (26), one can arrive at the limiting forms of $Y(x)$ as

$$Y(x) \approx x, \quad \text{for } x \rightarrow 0 (t' \rightarrow \infty, \ell_{\max} < \infty), \quad (27)$$

and

$$Y(x) = A, \quad \text{for } x \rightarrow \infty (t' < \infty, \ell_{\max} \rightarrow \infty). \quad (28)$$

Of course, it would again be interesting to learn about the full form of $Y(x)$.

Also, analogous to T_c^L in critical phenomena, one can define a finite-size equilibration time t_{eq}^L that is needed to reach ℓ_{\max} , as demonstrated in Fig. 4(a). Then one can write down a scaling equation analogous to (23) as

$$[\ell_{\max} - \ell_0] \sim t_{\text{eq}}^{L/3}. \quad (29)$$

This scaling behavior is demonstrated in Fig. 4(b), where we show plots of ℓ_{\max} versus t_{eq}^L on a logarithmic scale, in both $d = 2$ and $d = 3$. Consistency of the simulation data with the solid line of the form (29) confirms the validity of this approach. Note that in this figure, we did not subtract ℓ_0 and the corresponding microscopic time from the abscissa. As will be seen later, ℓ_{\max} for the systems considered here are significantly larger than ℓ_0 , so one does not expect a big difference after subtracting. Equation (29) is analogous to the one used to obtain the equilibrium dynamic critical exponent from simulations done at criticality [16], viz., the relaxation time $\tau \sim L^\zeta$.

III. SIMULATION RESULTS AND ANALYSIS

Having set the methodology in place, in this section we present results from the MC simulation of the Kawasaki-Ising model in $d = 2$ and 3, combined with the finite-size scaling analysis.

A. Results in $d = 2$

In Fig. 5, we present snapshots during the evolution of an Ising system, starting from a 50:50 random mixture of up and

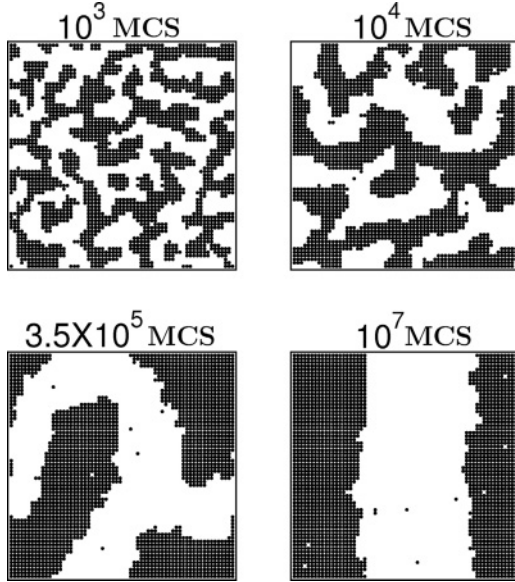


FIG. 5. Evolution snapshots from different times, as indicated, for the Kawasaki-Ising model in $d = 2$ at $T = 0.6T_c$. The last snapshot corresponds to a completely equilibrated configuration.

down spins, obtained via a MC simulation at temperature $T = 0.6T_c$. The times at which the shots were taken are mentioned on the figure. While the last snapshot corresponds to a situation when A and B phases are completely separated, the one at $t = 3.5 \times 10^5$ MCS represents the situation when the finite-size effect began to enter, which will be clear from our subsequent discussion.

From Fig. 4(a), by observing that the data for smaller systems are following the ones for larger systems almost all the way up to the saturation value, it is already evident that the finite-size effect is rather weak. However, for a quantitative statement and to gain detailed information about the growth exponent, more sophisticated analysis is called for. Following the discussion in the previous section, in Fig. 6 we plot $Y = [\ell(t') - \ell_0]/t'^\alpha$ as a function of $x/(x + x_0)$. Note that x_0 was introduced to see the behavior of Y properly both for small and large x . For convenience we set it to 5. In this exercise we have varied α and ℓ_0 (or the microscopic time t_0 associated with this length) to get the optimum collapse of data from different system sizes. In Fig. 6(a), where $\ell(t)$ is being used from Eq. (10), the optimum data collapse is obtained for $\ell_0 \simeq 4a$ (average cluster size after 20 MCS since quench), with a being the lattice spacing and $\alpha \simeq 0.33$. A similar exercise when $\ell(t)$ is being obtained from Eq. (12), as shown in Fig. 6(b), gives $\alpha \simeq 0.35$ and ℓ_0 there corresponds to the same number of MCS after quench. Note that ℓ_0 in our analysis is a bare length, independent of time, and the scaling behavior (25) will be obtained when this is chosen appropriately. These numbers, as expected, provides a constant value of $Y(x)$ in the region unaffected due to finite system size, which should be identified with the growth amplitude A for which we quote 0.29 ± 0.01 [cf. Fig. 6(a)]. The arrows in Fig. 6 marks the location where $Y(x)$ starts deviating from its constant value. The sharp nature of the crossover is indicative of only small size effects. Essentially, finite-size effects that can affect the

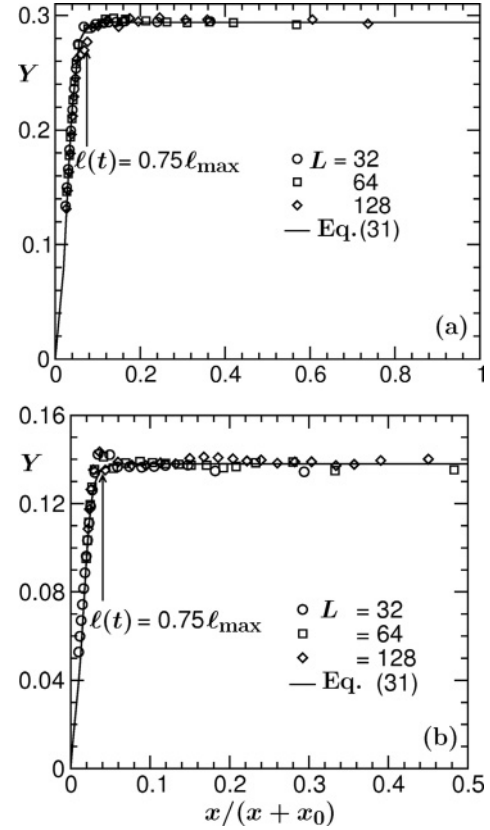


FIG. 6. (a) Finite-size scaling plot of Y , with $\ell_0 = 3.6$ lattice constants (after 20 MCS from the quench time) and $\alpha \simeq 0.33$, as a function of $x/(x + x_0)$, $x_0 = 5$. The continuous curve is a fit to Eq. (31), with the best fit parameters mentioned in the text. The arrow roughly marks the appearance of the finite-size effect. Note that the $\ell(t)$ data used here were obtained from Eq. (10). (b) Same as (a), but $\ell(t)$ were obtained from the first zero crossing of $C(r, t)$ [cf. Eq. (12)]. In this case, $\ell_0 \simeq 2.7$ lattice constants (at 20 MCS from quench) and $\alpha \simeq 0.35$.

observation of expected growth law, if not appropriately taken care of, appear very late, viz., when

$$\ell(t) = (0.75 \pm 0.05)\ell_{\max}, \quad (30)$$

which we quantified from the location of the arrow marks. Of course, this value is significantly large compared to the earlier understanding and expectation. Note that the snapshot at $t = 3.5 \times 10^5$ MCS in Fig. 5 corresponds to this length.

In an attempt to learn the full form of $Y(x)$, we construct the following functional form:

$$Y(x) = \frac{Ax}{x + 1/(p + qx^\beta)}, \quad (31)$$

that has limiting behaviors consistent with (27) and (28). The continuous lines in Figs. 6(a) and 6(b) are fits to the form (31), with

$$A \simeq 0.29, \quad p \simeq 3, \quad q \simeq 6400, \quad \beta = 4, \quad (32)$$

and

$$A \simeq 0.14, \quad p \simeq 7, \quad q \simeq 13700, \quad \beta = 4, \quad (33)$$

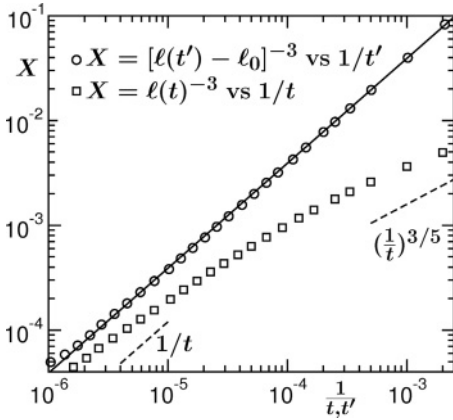


FIG. 7. Plot of $[\ell(t') - \ell_0]^{-3}$ vs. $1/t'$, and $\ell(t)^{-3}$ versus $1/t$, for $L^2 = 64^2$, with $\ell(t)$ being calculated from Eq. (10). The continuous line has slope $39 = 1/A^3$.

and thus have the convergence

$$(x \rightarrow \infty)Y(x) \approx A(1 - fx^{-n}), \quad n = 5. \quad (34)$$

Of course, the possibility of an exponential correction cannot be ruled out. This may be compared with a much slower convergence of such function in dynamic critical phenomena [47]. Note that the understanding of the finite-size effect in both equilibrium and nonequilibrium dynamics is a nontrivial task and significant attention is called for.

A direct view of what happens after the corrective measure has been taken, in terms of subtraction of ℓ_0 , is shown in Fig. 7 where we plot $[\ell(t') - \ell_0]^{-3}$ versus $1/t'$, and $\ell(t)^{-3}$ versus $1/t$, for $L = 64$. A logarithmic scale was used to bring visibility to a wide range of data. The linear behavior of the data after subtracting ℓ_0 , starting from the very early time, justifies the introduction of ℓ_0 again. The continuous line there is a plot of the form $\bar{A}x$ with $\bar{A} \simeq 39 = 1/A^3$. On the other hand, notice the strong curvature when ℓ_0 is not subtracted. The dashed lines marked by $1/t$ and $(\frac{1}{t})^{3/5}$ on this figure correspond to $\ell(t) \sim t^{1/3}$ and $t^{1/5}$, respectively. Thus, when ℓ_0 is not appropriately subtracted, by only observing the trend on a log-log plot, one may be misled to conclude that there is a gradual crossover from one regime to the other. Even though a surface-diffusion dominated regime leading to $t^{1/4}$ growth appears to be missing at this temperature, it remains to be checked at lower temperature. (See Ref. [48] for a discussion of a crossover from $t^{1/4}$ to $t^{1/3}$.) Note that the exercise here, as well as the one in Fig. 6, where Y is very flat from very early time all the way to the moment when the finite-size effect enters, is already indicative of the absence of any strong corrections to scaling.

Before moving ahead for another proof of the evidence for the absence of negligible corrections to scaling, we first show the scaling plot of $C(r, t)$ in Fig. 8, where good quality data collapse is obtained starting from the very beginning until $t = 3 \times 10^5$ MCS, when the finite-size effect begins. Next we introduce a length ℓ_s to write

$$\ell'(t') = \ell(t') - \ell_s = [\ell_0 - \ell_s] + At'^\alpha, \quad (35)$$

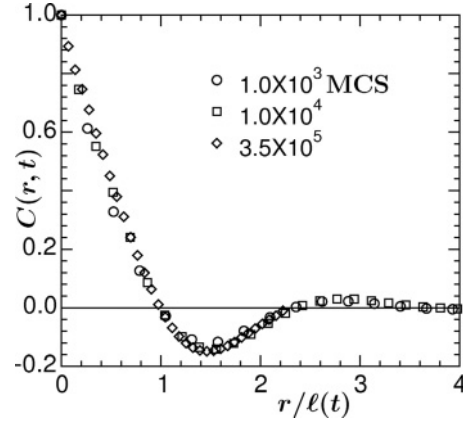


FIG. 8. Scaling plot of $C(r, t)$ at $T = 0.6T_c$. Note that $\ell(t)$ was obtained using Eq. (10).

and calculate the instantaneous exponent [20]

$$\alpha_i = \frac{d[\ln \ell'(t')]}{d[\ln t']}, \quad (36)$$

to obtain

$$\alpha_i = \alpha \left[1 - \frac{\ell_0 - \ell_s}{\ell'(t')} \right]. \quad (37)$$

In accordance with Eq. (37), when α_i is plotted as a function of $1/\ell'(t')$, for $\ell'(t') > 0$, one expects the linear behavior with a y intercept equal to α . Figure 9(a) shows such plots for $\ell_s = 0.0, 3.6$, and 5.0 , as indicated. The dashed lines have a y intercept, $\alpha = 1/3$, and slopes

$$m = -\frac{\ell_0 - \ell_s}{3}. \quad (38)$$

In this exercise essentially we have, by force, invoked different initial lengths into the average domain size, which results in different slopes in the instantaneous exponent when plotted versus inverse length. The consistency of the slopes with (38) (represented by dashed lines) is interesting. Particularly the behavior of α_i for $\ell_s = 3.6$ again speaks to the choice of ℓ_0 and indicates that the LS scaling regime is realized very early. In Fig. 9(b), we present results with $\ell_s = 3.6$ for various system sizes $L^2 = 16^2, 32^2$, and 64^2 . In all of the cases, α_i oscillates around $1/3$. This observation, using a system size as small as $L^2 = 16^2$, stresses against the unnecessary attempt to simulate larger systems.

This result is in strong disagreement with the earlier [20] understanding of domain coarsening, in a $2-d$ conserved Ising model for critical quench, that α is strongly time dependent and the LS value is recovered only asymptotically as $\ell(t) \rightarrow \infty$. The route to this finite-time correction was thought to be an additional term, $\propto 1/\ell(t)^3$, in Eq. (5) [cf. Eq. (9)], accounting for an enhanced interface conductivity. Note that the term $\propto 1/\ell(t)^3$ could also be motivated by introducing a curvature dependence in σ as

$$\sigma[\ell(t)] = \frac{\sigma(\infty)}{1 + \frac{2\delta}{\ell(t)}}, \quad (39)$$

with δ being the Tolman length [49]. However, our observation of a negligible correction to the exponent, starting from the very early time, is consistent with the growing evidence [50,51]

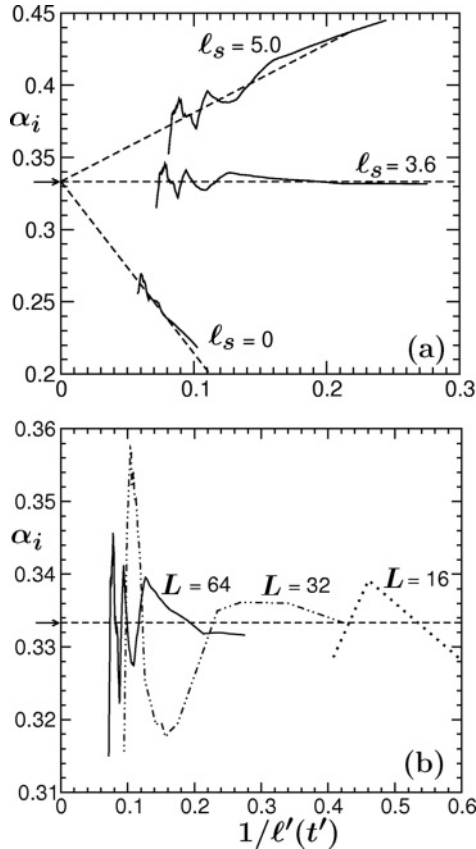


FIG. 9. (a) Plot of instantaneous exponent α_i as a function of $1/\ell'(t')$ for three different choices of ℓ_s as indicated, with $L^2 = 64^2$. The dashed straight lines have slopes $-1.19, 0$, and 0.49 , respectively. (b) Plot of α_i vs. $1/\ell'(t')$ for $\ell_s = 3.6$ and $L^2 = 16^2, 32^2$, and 64^2 . In both (a) and (b), the arrows on the ordinate mark the value $\alpha = 1/3$. Note that $\ell(t)$ was calculated from Eq. (10). All data sets correspond to averaging over 1000 independent initial conditions.

that the Tolman length is absent in a symmetrical model [52], where the leading correction is of a higher order. Also, small corrections that may be present, coming from the curvature dependence of the kinetic prefactor in Eq. (5), is beyond the accuracy of data in the present work. On the other hand, for a 50:50 composition, since the domain boundaries are essentially flat starting from very early time, any curvature dependence is expected to be absent. Thus, we conclude that this misunderstanding about the strong time dependence in α was due to the presence of a time-independent length ℓ_0 in $\ell(t)$, which our analysis subtracts out in an appropriate way.

B. Results in $d = 3$

In this subsection, we turn our attention to the kinetics of phase separation in $d = 3$. Figure 10 shows 3- d snapshots of the time evolution of the Kawasaki-Ising model at four different times, as indicated on the figure where the last snapshot is clearly seen to have been equilibrated. Analogous to $d = 2$, all results presented here were obtained at $T = 0.6T_c$, with $T_c = 4.51k_B T/J$ in this case, and the composition was chosen to be 50:50 as well.

In Fig. 11(a), we present direct plots of $\ell(t)$ as a function of t , for $L^3 = 16^3, 32^3$, and 64^3 , where $\ell(t)$ was calculated

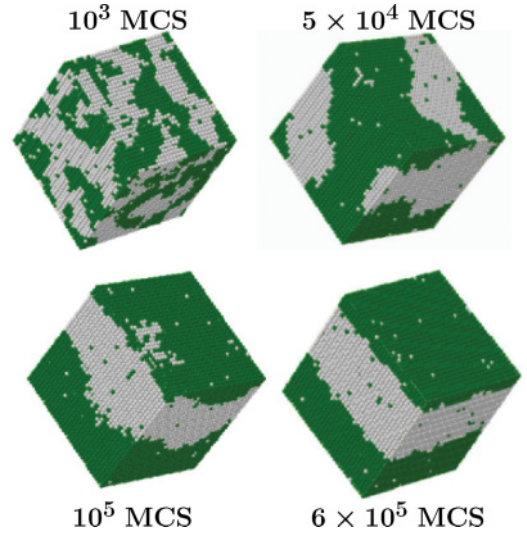


FIG. 10. (Color online) Evolution snapshots from different times for a 3- d Ising model with $L^3 = 32^3$ and $T = 0.6T_c$. A and B particles are marked dark green and light gray, respectively.

from Eq. (12). Again, the finite-size effects look to be small. In Fig. 11(b), we present a plot of $Y(x)$, using the data in Fig. 11(a), as a function of $x/(x+x_0)$, $x_0 = 5$. The best data collapse in this case was obtained for $\ell_0 = 2.5$ [10 MCS after the quench; note that the corresponding value of ℓ_0 from Eq. (10) is 3.0 and $\alpha \simeq 0.315$] and $\alpha \simeq 0.35$. The very flat behavior of $Y(x)$, starting from the beginning again, speaks to the absence of any strong correction to the growth law. However, compared to the $d = 2$ case, one may expect a slightly stronger correction here because of the inherent curvature present in the cylinder-like domain objects, as opposed to the stripelike structures in $d = 2$. Possibly because of that, we could not obtain a good collapse of the data from $L^3 = 16^3$ on top of the ones presented, since the whole data set for $L^3 = 16^3$ is from very early time and suffers from corrections. The onset of the finite-size effect, as obtained from the arrow mark where $Y(x)$ deviates from the flat behavior, is in quantitative agreement with the two-dimensional situation, as quoted in Eq. (30). Here also the third snapshot in Fig. 10 (at $t = 10^5$ MCS) is presented at this onset. A fitting, shown by the continuous line, to the form (31) ($A = 0.24$, $p \simeq 4$, $q \simeq 13050$, and $\beta = 4$), again is consistent with asymptotic convergence (34).

In Fig. 12(a), we present the instantaneous exponent α_i as a function of $1/\ell'(t')$ for $L^3 = 64^3$ and three choices of ℓ_s , as indicated. In all the cases, the exponent fluctuates around the mean value 0.34. Note that α estimated from $S(k, t)$ and $P(\ell_d, t)$ are slightly higher and lower, respectively, compared to the one presented.

The appearance of growing oscillation in α_i , seen in Figs. 9 and 12, around the mean value is due to a lack of statistics and was also pointed out by Shinozaki and Oono [30]. The results could be made smoother by considering a bigger system size [see Fig. 9(b)] or averaging over a large number of systems [Fig. 12(b)]. In a finite system, as time increases, for an extended period of time, two large neighboring domains of the same sign may not merge, thus lowering the value of α . After a long time, when two large domains merge, it results in a drastic

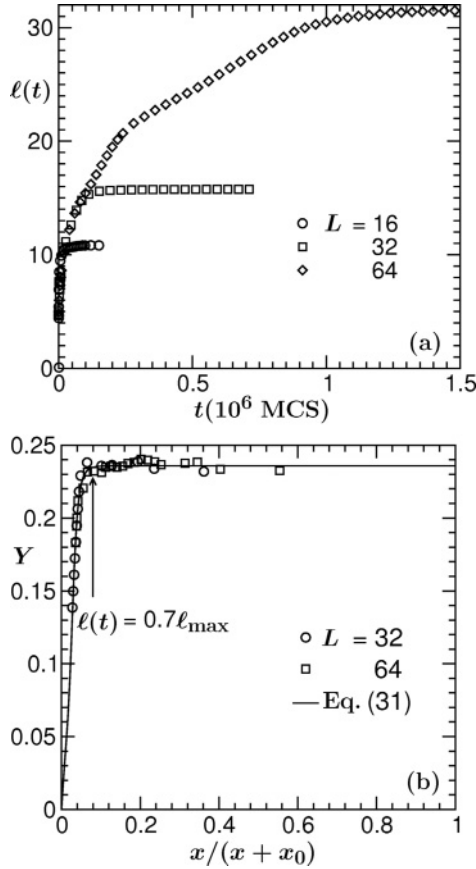


FIG. 11. (a) Plot of $\ell(t)$ obtained from the first zero crossing of $C(r,t)$ vs. t for the systems $L^3 = 16^3$, 32^3 , and 64^3 . (b) Finite-size scaling plot of Y for the data presented in (a) vs. $x/(x+x_0)$ with $x_0 = 5$. Here $t_0 = 10$ (10 MCS from the quench) and $\alpha = 0.35$. Appearance of the finite-size effect, obtained from the arrow mark, is estimated to be at $\ell(t) \simeq 0.7\ell_{\max}$, which is in close agreement with the one for $d = 2$.

enhancement in the value of α . This character is in fact visible in the direct plot of $\ell(t)$ versus t at late times [cf. $L = 128$ in Fig. 4(a) and $L = 64$ in Fig. 11(a)]. Note that this oscillation could be a route to an error if one obtains α from least square fitting without choosing the range appropriately. Finally, it will be interesting to know the temperature dependence of ℓ_0 and amplitude A as well as of finite-size effects. All these, however, we leave for future work.

IV. SUMMARY

This paper contains a comprehensive study of domain coarsening in a phase-separating system with diffusive dynamics in $d = 2$ and $d = 3$. Various ways of analysis give results for a growth law consistent with the expected LS exponent $\alpha = 1/3$. As opposed to the earlier understanding, correction appears to be very weak, thus LS scaling behavior is realized very early. A weak finite-size effect is a welcome message, which is suggestive of avoiding large systems, and instead focusing on accessing the long-time scale, which often is necessary for systems exhibiting multiple scaling regimes.

Our observation should be contrasted with an earlier study of Heermann *et al.* [9] that reports a very strong finite-size

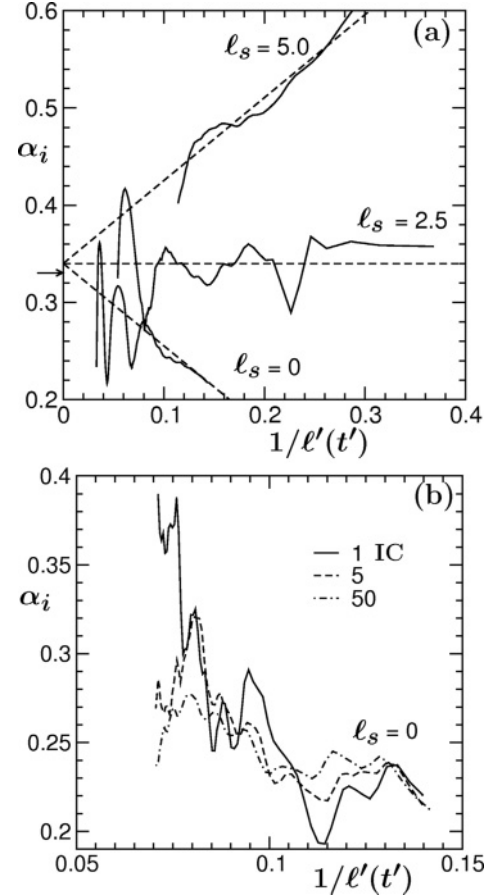


FIG. 12. (a) Plot of instantaneous exponent α_i vs. $1/\ell'(t')$ with three different values of $\ell_s = 0, 2.5$, and 5 . The dashed lines correspond to $\alpha = 0.34$. The arrow on the ordinate marks the value $\alpha = 1/3$. The data presented here correspond to $L = 64$ and were obtained from averaging over 150 initial configurations. (b) Plot of α_i vs. $1/\ell'(t')$ for $\ell_s = 0$, showing a reduction of noise when averaged over a larger number of initial configurations (IC).

effect. However, this latter study was based on an extremely off-critical composition and should not be considered to have general validity. Note that due to the expected presence of correction in such off-critical composition, where dropletlike structures form with a finite radius of curvature at early time, the analysis is more difficult. Also, one should be prepared to encounter a stronger size effect in more complicated situations, e.g., systems exhibiting anisotropic patterns [35–39,41,42].

One may of course ask if the small finite-size effect observed for diffusive dynamics is also valid for the kinetics of phase separation in fluids. A comprehensive study in that direction, for both binary- and single-component fluids, is in progress. In fact, preliminary findings from these latter studies are suggestive of a more general validity of the results presented here. Such studies are important since the brute force method of simulating very large systems, particularly for the study of fluid phase separation via MD simulation, is not often helpful to access long-time scales, even with the present day high speed computers, and thus may not result in a very conclusive understanding.

A deeper understanding of ℓ_0 requires further study; particularly, how the system is led to instability is a

fundamental question to be asked. Studies with different initial configurations and quenching to different temperatures should be able to provide a better understanding of this quantity. Even though scaling corrections appear to be negligible for critical quench due to the flat nature of the domain boundaries, one expects corrections for off-critical composition. This expected correction coming from surface tension should be of a higher order than the linear one for a symmetric model. On the other hand, it would be interesting to learn about the leading order correction coming from the kinetic prefactor.

Finally, we expect the observations, understanding, and finite-size scaling technique used in this work to find relevance in other, systems exhibiting growing length scales, e.g.,

ordering in ferromagnets, surface growth, clustering in cooling granular gas, dynamic heterogeneity in glasses, etc. In line with this work, many earlier studies on domain coarsening may need to be revisited for a better understanding, which was not possible because of a lack of reliable methods of analysis.

ACKNOWLEDGMENTS

S.K.D. is grateful to K. Binder for useful discussions. The authors acknowledge financial support via Grant No. SR/S2/RJN-13/2009 from the Department of Science and Technology, India. S.M. also acknowledges the Council of Scientific and Industrial Research, India, for financial support.

-
- [1] A. J. Bray, *Adv. Phys.* **51**, 481 (2002).
 [2] K. Binder, in *Phase Transformation of Materials*, edited by R. W. Cahn, P. Haasen, and E. J. Kramer, Mater. Sci. Technol., Vol. 5 (VCH, Weinheim, 1991), p. 405.
 [3] *Kinetics of Phase Transitions*, edited by S. Puri and V. Wadhawan (CRC, Boca Raton, 2009).
 [4] I. M. Lifshitz and V. V. Slyozov, *J. Phys. Chem. Solids* **19**, 35 (1961).
 [5] E. D. Siggia, *Phys. Rev. A* **20**, 595 (1979).
 [6] H. Furukawa, *Phys. Rev. A* **31**, 1103 (1985); **36**, 2288 (1987).
 [7] M. E. Fisher in *Critical Phenomena*, edited by M. S. Green (Academic, London, 1971), p. 1.
 [8] *Finite Size Scaling and the Numerical Simulations of Statistical Systems*, edited by V. Privman (World Scientific, Singapore, 1990).
 [9] D. W. Heermann, L. Yixue, and K. Binder, *Physica A* **230**, 132 (1996).
 [10] J. Viñals and D. Jasnow, *Phys. Rev. B* **37**, 9582 (1988).
 [11] S. Majumder and S. K. Das, *Phys. Rev. E* **81**, 050102(R) (2010).
 [12] K. Binder, *Phys. Rev. B* **15**, 4425 (1977).
 [13] K. Binder and H. L. Frisch, *Z. Phys. B* **84**, 403 (1991).
 [14] K. Kawasaki, in *Phase Transition and Critical Phenomena*, edited by C. Domb and M. S. Green (Academic, New York, 1972), Vol. 2, p. 443.
 [15] R. A. L. Jones, *Soft Condensed Matter* (Oxford University Press, Oxford, 2008).
 [16] D. P. Landau and K. Binder, *A Guide to Monte Carlo Simulations in Statistical Physics* (Cambridge University Press, Cambridge, 2005).
 [17] D. Frankel and B. Smit, *Understanding Molecular Simulations: From Algorithms to Applications* (Academic, San Diego, 2002).
 [18] T. M. Rogers and R. C. Desai, *Phys. Rev. B* **39**, 11956 (1989).
 [19] J. F. Marko and G. T. Barkema, *Phys. Rev. E* **52**, 2522 (1995).
 [20] D. A. Huse, *Phys. Rev. B* **34**, 7845 (1986).
 [21] J. G. Amar, F. E. Sullivan, and R. D. Mountain, *Phys. Rev. B* **37**, 196 (1988).
 [22] C. Roland and M. Grant, *Phys. Rev. Lett.* **60**, 2657 (1988).
 [23] C. Roland and M. Grant, *Phys. Rev. B* **39**, 11971 (1989).
 [24] S. K. Das and S. Puri, *Phys. Rev. E* **65**, 026141 (2002).
 [25] A. Milchev, K. Binder, and D. W. Heermann, *Z. Phys. B* **63**, 521 (1986).
 [26] C. Roland and M. Grant, *Phys. Rev. Lett.* **63**, 551 (1989).
 [27] M. Rao, M. H. Kalos, J. L. Lebowitz, and J. Marro, *Phys. Rev. B* **13**, 4328 (1976).
 [28] G. S. Grest and D. J. Srolovitz, *Phys. Rev. B* **30**, 5150 (1984).
 [29] G. F. Mazenko, O. T. Valls, and F. C. Zhang, *Phys. Rev. B* **31**, 4453 (1985); **32**, 5807 (1985).
 [30] A. Shinozaki and Y. Oono, *Phys. Rev. E* **48**, 2622 (1993).
 [31] M. Laradji, S. Toxavaerd, and O. G. Mousitsen, *Phys. Rev. Lett.* **77**, 2253 (1996).
 [32] A. K. Thakre, W. K. den Otter, and W. J. Briels, *Phys. Rev. E* **77**, 011503 (2008).
 [33] H. Kabrede and R. Hentschke, *Physica A* **361**, 485 (2006).
 [34] S. Ahmad, S. K. Das, and S. Puri, *Phys. Rev. E* **82**, 040107 (2010).
 [35] S. K. Das, S. Puri, J. Horbach, and K. Binder, *Phys. Rev. E* **72**, 061603 (2005); *Phys. Rev. Lett.* **96**, 016107 (2006); *Phys. Rev. E* **73**, 031604 (2006).
 [36] S. J. Mitchell and D. P. Landau, *Phys. Rev. Lett.* **97**, 025701 (2006).
 [37] K. Bucior, L. Yelash, and K. Binder, *Phys. Rev. E* **77**, 051602 (2008).
 [38] L. Yelash, P. Virnau, W. Paul, K. Binder, and M. Müller, *Phys. Rev. E* **78**, 031801 (2008).
 [39] K. Bucior, L. Yelash, and K. Binder, *Phys. Rev. E* **79**, 031604 (2009).
 [40] S. K. Das, J. Horbach, and K. Binder, *Phys. Rev. E* **79**, 021602 (2009); *Mod. Phys. Lett. B* **23**, 549 (2009).
 [41] M. J. A. Hore and M. Laradji, *J. Chem. Phys.* **132**, 024908 (2010).
 [42] K. Binder, S. Puri, S. K. Das, and J. Horbach, *J. Stat. Phys.* **138**, 51 (2010).
 [43] A. Sicilia, J. J. Arenzon, A. J. Bray, and L. F. Cugliandolo, *Phys. Rev. E* **76**, 061116 (2007).
 [44] A. Sicilia, Y. Sarrazin, J. J. Arenzon, A. J. Bray, and L. F. Cugliandolo, *Phys. Rev. E* **80**, 031121 (2009).
 [45] A. J. Bray and S. Puri, *Phys. Rev. Lett.* **67**, 2670 (1991).
 [46] Y. Oono and S. Puri, *Mod. Phys. Lett. B* **2**, 861 (1988).
 [47] S. K. Das, M. E. Fisher, J. V. Sengers, J. Horbach and K. Binder, *Phys. Rev. Lett.* **97**, 025702 (2006); S. Roy and S. K. Das, *EPL* **94**, 36001 (2001).
 [48] S. Puri and Y. Oono, *Phys. Rev. A* **38**, 1542 (1988).
 [49] R. C. Tolman, *J. Chem. Phys.* **17**, 333 (1949).
 [50] D. Winter, P. Virnau, and K. Binder, *J. Phys. Condens. Matter* **21**, 464118 (2009).
 [51] B. J. Block, S. K. Das, M. Ottel, P. Virnau, and K. Binder, *J. Chem. Phys.* **133**, 154702 (2010).
 [52] M. P. A. Fisher and M. Wortis, *Phys. Rev. B* **29**, 6252 (1984).